Electrokinetic microfluidic devices for rapid, low power drug delivery in autonomous microsystems†

Aram J. Chung,[a] Donn Kim[b] and David Erickson*[a]

Received 30th August 2007, Accepted 29th November 2007
First published as an Advance Article on the web 14th December 2007
DOI: 10.1039/b713325a

In this work, a low power and robust electroactive microwell-based implantable drug delivery system, intended for use with autonomous microsystems, is presented. The device comprises of an upper silicon based structure in which the drug storage sites are defined and a lower electrically functionalized PDMS (polydimethylsiloxane) backing. The drug ejection mechanism developed here exploits localized electrokinetic effects to control both the release time and release rate of chemicals stored in independent well sites. It is shown how this can reduce the dosage time from hours to seconds over previous diffusion based approaches, using as little as 20 mJ of energy per dose. This paper focuses on presenting the design and characterizing the electrokinetic transport mechanics which govern the release time and dispersal pattern of the well contents using a series of experimental and numerical techniques.

Introduction

Autonomous microsystems can be defined as ''systems, enabled through microfabrication technology, that function of their own accord with the ability to interpret and interact with their environment''. Recent developments in micro-electro-mechanical-systems or MEMS[1,2] component-level technology (including power generation,[3] energy storage, communications, sensing, and subcomponent assembly) have brought the development of such systems closer to a reality. While many of the initial thrusts into this field were directed towards autonomous sensor networks,[4] the integration of bioMEMS[5–8] and microfluidic elements[9–12] in these types of devices is increasingly finding application to *in vitro* and, in particular *in vivo*, medical devices (mostly through various ''smart-pill'' type technologies).[13,14] While such systems are becoming increasingly functional, their primary use remains diagnostic rather than therapeutic. One of the limitations of these devices, and all autonomous microsystems, is that the power load is relatively large compared with the amount of energy available from current battery technology. This tends to significantly limit the lifetime of the device.

Oral, nasal, intravenous, pulmonary and transdermal methods represent the traditional and often preferred routes for drug delivery. Broadly speaking, the advantage of the former of these is its relative simplicity, while the later methods have been developed to enable more rapid delivery and better specific organ targeting.[15] The advantages that emerging MEMS based implantable drug delivery systems offer over these conventional methods are controllability (*i.e.* the ability to autonomously deliver very precise doses, either periodically or in response to a sensor event), delivery speed and microscopic localization.[16,17] Such capabilities could have significant impact on future human health.[18]

Current implantable drug delivery systems[19–21] can be categorized as either passive or active.[16] Passive systems are based on chemical release beginning immediately after implantation (either through a diffusive processes or mechanical pumping) and continuing until the ''on-board'' dose is depleted. Though this offers control over the total dose, neither the delivery timing nor its rate can be manipulated by the physician, patient or the system itself.[16]

One of the first experimental demonstrations of an active drug delivery was described by Santini *et al.*[22–24] In their system, an array of individually sealed reservoirs were fabricated on a silicon microchip and filled with a series of different chemicals. The system could then be implanted and the contents of each reservoir released by applying an external electric potential (which induced electrochemical dissolution of the gold sealing membrane). This active control over the delivery timing and dosage can have a significant effect on its therapeutic efficacy in that the specific drug and its dosage can be released rapidly in consideration of the patients' current condition. Such systems have the advantage of a relatively simple construction, requiring only low voltage electrical actuation as opposed to mechanical pumping.

Drug release from self-contained reservoirs rely on a diffusive transport mechanism. This allows for continuous releases of contents over an extended period of time, which could take several hours to days depending on the diffusion coefficient of the chemical.[22–24] Thus, while the dose initiation time can be manipulated, the delivery rate remains fixed to this relatively slow rate. In certain cases it is desirable to possess greater control over the release rate to allow for a more rapid dosage (in order to better respond to the patient's condition)

[a]*Sibley School of Mechanical and Aerospace Engineering, Cornell University, Ithaca, NY, 14853, USA. E-mail: de54@cornell.edu; Fax: +1 607-255-1222; Tel: +1 607-255-4861*
[b]*School of Electrical and Computer Engineering, Cornell University, Ithaca, NY, 14853, USA*

† Electronic supplementary information (ESI) available: One supplementary video (movie1.wmv) that illustrates the electrokinetically enhanced ejection of the contents from the well. Another video shows the recirculation effect described below (movie2.wmv). See DOI: 10.1039/b713325a

or to better mimic a physiological release profile. For example, insulin and other hormones are well-known to be secreted by the body in a pulsatile manner. Deficiency in hormones of the anterior pituitary gland, such as thyroid stimulating hormone, growth hormone, luteinizing hormones regulated by the hypothalamus may lead hypothyroidism (insufficient production of thyroid hormone), hypoglycemia/dwarfism (inadequate production of growth hormone) or hypogonadism (failure of gonadal function). Pulsatile administration of small volumes of thyroid releasing hormone, growth hormone releasing hormone[24] and gonadotropin releasing hormone[24] can help the severity of these deficiencies.

In this work, we present an electroactive microwell[25] based drug/chemical delivery system which provides this active chip control over the delivery rate, timing and speed without the need for significant additional on-chip architecture or large power consumption. A series of single and multiple well chips were fabricated, all of which used the two component construction. As shown in Fig. 1, the silicon layer contained the drug well(s) and the upper set of electrodes, while the PDMS layer served to seal the well and hold the lower electrode. The device structure is a modification of that presented by Santini *et al.*,[22] exploiting the same electrochemical dissolution technique to expose the contents, but incorporating electrical functionality onto a flexible PDMS backing to enable control over the electrokinetic transport. As will be described below, the technique is based on exploiting highly localized electrokinetic transport to rapidly exchange the contents of the well with the external environment. This allows for a controlled reduction in the total dosage time to seconds rather than hours, as will be demonstrated. Here we focus on presenting the overall design and construction of the device, and detailing the delivery rate and drug dispersion pattern as a function of the strength of the applied electric field. A detailed 3D finite element analysis of the transport dynamics of the system is conducted in order to better understand the governing mechanisms behind the ejection process. As alluded to above, this device is designed for use in autonomous microfluidic systems and thus a detailed analysis of the voltage, power and energy requirements is also conducted.

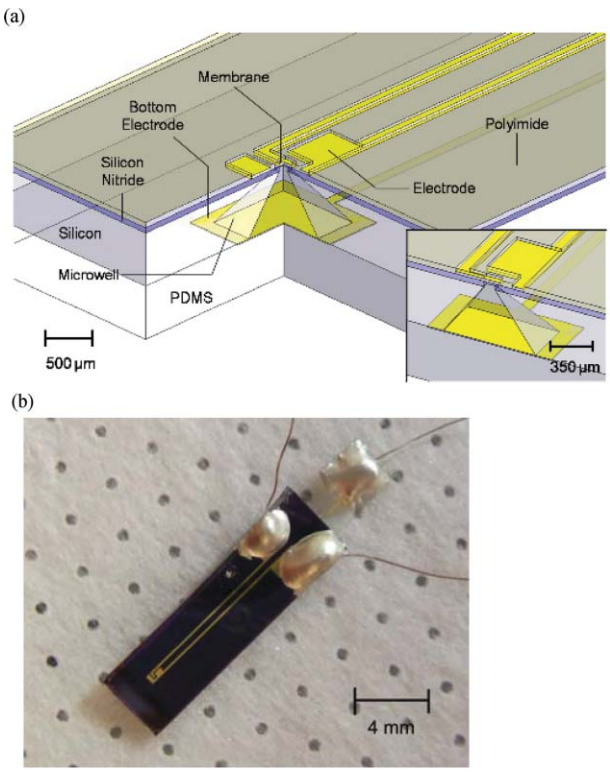

Fig. 1 (a) Schematic representative section of an electroactive microwell drug delivery system developed here. Inset: cross sectional view of the system. (b) Fabricated and assembled device with electrical leads connected to thin copper wires.

Materials and methods

In this materials and methods section we begin with a detailed description of the device fabrication and assembly procedure (a detailed process diagram of the fabrication and assembly procedure is also included in the electronic supplementary information†). The final two subsections describe the device operation and experimental procedure.

Microfabrication

In our device we have used double side polished, (100) *n*-doped silicon wafers with a thickness of 500 μm. In general, thicker wafers were preferred in order to maximize the well volume. To fabricate the devices, we first used low pressure chemical vapour deposition (LPCVD) to deposit a 200 nm thick layer of silicon nitride on both sides of the wafer. 760 μm squares were then reactive ion etched into the back side silicon nitride layer defining the eventual location of the wells. Following this, a 300 nm layer of gold was evaporated and patterned using image reversal contact lithography process on the top surface to form the electrode leads and well membrane. A polyimide (Durimide®) passivation layer was then deposited on the topside of the wafer, which served to electrically isolate the electrodes from the electrolyte solution during membrane dissolution. The passivation layer was patterned using an aluminium mask and oxygen plasma etching process, so that only the eventual location of the membrane and surrounding C-shape gold features would be exposed to the solution (see Fig. 2c). The microwells were then defined by immersing the wafer in KOH for roughly 8 h. During this process, the exposed silicon was etched along the crystal plane, resulting in the square pyramidal shape shown in Fig. 1a. Lastly, the remaining nitride on the backside of the wafer and underneath the gold membrane was etched by reactive ion etching. The resulting drug wells were 760 μm square at the base and 52 μm square at the top, resulting in a total cavity volume of approximately 100 nL.

To create the lower gold patterned PDMS layer we used a similar technique to that described by Lee *et al.*[26] 100 nm thick gold features were first patterned on a silicon substrate. After the gold features were created, an MPTMS (3-mercaptopropyl-trimethoxysilane) film was deposited onto the top surface of the wafer using molecular vapour deposition (MVD). The MPTMS layer served as an organic adhesion layer aiding with the transfer of the gold features from the silicon wafer to the

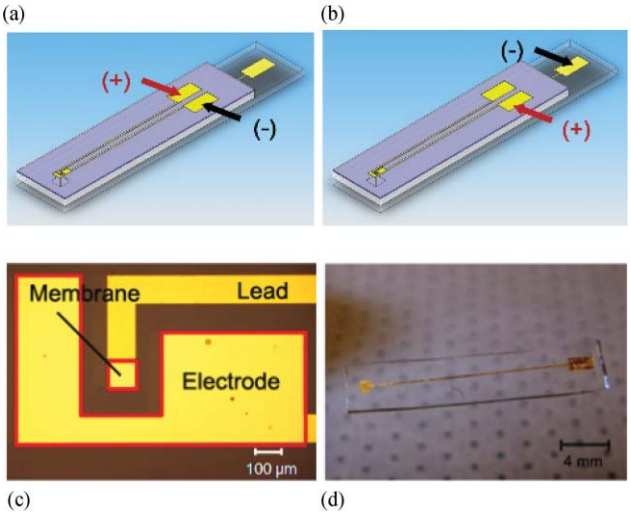

Fig. 2 System operation. (a) Stage 1: to electrochemically dissolve the membrane a potential is applied between the two upper electrodes. (b) Stage 2: after dissolution to eject the contents, the potentials applied between the upper electrode and the lower one on the PDMS. (c) Magnified view of microchip from above looking at the region near the membrane. Pale yellow regions (membrane and C-shape gold features) are gold where the polyimide layer was etched. (d) An example of gold–PDMS bottom substrate.

PDMS.[27] After surface modification, a 5 : 1 (base : linker) mixture of PDMS was spin coated at 100 rpm for 30 s onto the wafer to a final thickness of approximately 580 μm. The PDMS was then cured at 80 °C for 90 min and the final structures were cut out of the mold (Fig. 2d).

Microchip assembly

The microwell reservoir was filled with a phosphate buffered saline (PBS) using 36G blunt syringe (NanoFil™, World Precision Instrument). A PBS buffer solution concentrated such that it had a similar chloride ion concentration to that found in human sera[28] was used here. For the flow visualization experiments, 1.9 μm fluorescent polystyrene microspheres (Duke Scientific) were added to the PBS solution. Once filled, the upper (silicon) and the bottom (PDMS) substrates were placed in conformal contact with each other and bonded together.

The use of a PDMS substrate greatly facilitated robust sealing of the device. In general, as long as wells were not overfilled, the conformal contact the PDMS formed with the polished bottom of the silicon microchip was sufficient to ensure a watertight seal. Significant overfilling of the wells tended to result in bursting of the gold membrane when the PDMS backing was applied. This is a result of the liquid being largely incompressible and thus very little overfilling was required in order to increase the internal pressure above that of the membrane burst pressure. To avoid this here, we slightly under filled the wells (leaving a small compressible air pocket).

Detailed device operation

Device operation occurs in two stages. As shown in Fig. 2a, in the first stage the potential is applied between two electrode pads on top of the microchip serving to electrochemically dissolve the membrane,[29] exposing the contents to the external environment (this was similarly demonstrated by Santini *et al.*[22]). To electrokinetically eject the contents from the well, in the second stage a potential field is applied between one of the upper electrodes and that on the PDMS at the bottom of the well, as illustrated in Fig. 2b. The application of this DC voltage (between 3–4 volts) over the relatively small wafer thickness results in extremely high electric field strength (just under 10^5 V m^{-1}) localized in the well.[25] As will be characterized in detail below, the resulting electrokinetic transport dramatically reduced the amount of time required to eject the contents of the well over diffusive transport[22–24] (from hours to minutes) with very little energy consumption. In all cases a Hewlett–Packard 6234A dual output power supply was used to apply these potentials and a Keithley 236 SMU (Source-Measure Unit) was used to record the current load. The transport of the microspheres was recorded using Unibrain Fire-i™ software and a Sony XCD-X710 camera.

Biocompatibility

Although the focus of this paper is on device design and transport analysis, it is important to briefly discuss the biocompatibility of the architecture introduced here. In a recent paper, Voskerician *et al.*[30] reported on the *in vivo* biocompatibility and biofouling of many of the fabrication materials used here (*i.e.* gold, silicon nitride, silicon) in the context of similar microsystem drug delivery devices. In general, it was found that of these materials, silicon was the least biocompatible, though it can undergo a number of simple surface passivation processes, such as silanation, to improve its performance. For the remaining materials used here, Richardson *et al.*[31] and Belanger and Marois[32] have reported polyimide and PDMS respectively as exhibiting good biocompatibility.

Results and discussions

The electroactive microwell drug delivery system described here allows the well contents to be stored indefinitely until a dose command is given, after which it can be rapidly released. As mentioned above, the use of an electrochemical membrane dissolution technique to expose the contents of a microwell to the external environment was previously demonstrated by Santini *et al.*[22] In the following two subsections, therefore, we focus on characterizing the novel aspects of the device reported here, namely, the electrokinetically enhanced ejection and low power operation consumption.

For completeness, however, we report that for our device a 5.0 V dc bias was applied between the upper electrodes, as shown in Fig. 2a, in order to initiate membrane dissolution. At this potential, the resulting electrochemical reaction required 6 to 7 s to release the membrane, exposing the well contents to the external environment. Lower biases resulted in much longer membrane release times. Further details on the process are available in the "Power consumption" section below.

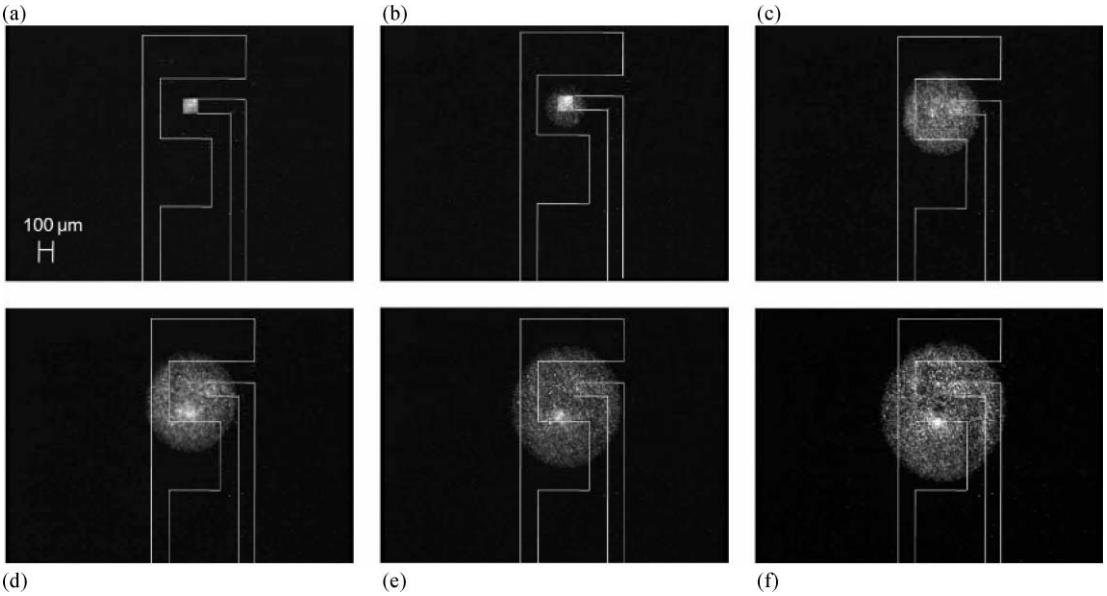

Fig. 3 Time lapse illustrating repulsion the ejection of 1.9 μm fluorescent polystyrene microsphere particles from an electroactive microwell. (a) After dissolution of the membrane, the fluorescent particles can be seen in the well. White lines outline the gold electrodes features. (b)–(f) frames taken every 2 s (total of 10 s) after application of a 4.0 V potential.

Electrokinetically enhanced ejection

Immediately following dissolution of the membrane, the applied potential field is switched to the configuration shown in Fig. 2b (*i.e.* between the upper and lower electrodes) and the resulting electrokinetic transport ejects the stored contents from the well to the external environment. Time lapse images in Fig. 3 illustrate the effect for the case of an applied potential of 4.0 V using the fluorescent flow tracers described above (see movie in the electronic supplementary information†). As can be seen, the process results in an approximately radial dispersal pattern. To characterize the dispersal pattern as a function of applied potential, the maximum dispersal radius was recorded as a function of time for 3.0 V, 3.5 V, 3.75 V and 4.0 V, respectively. These measurements were performed using a similar set of images to those shown in Fig. 3, which were processed using ImageJ (http://rsb.info.nih.gov/ij/) and a self-written MATLAB routine (Mathworks, Natick, MA, USA). This range of applied potentials was used as they represent an optimal between expected ejection time[25] and power consumption (which will be characterized in the following section).

The results of these experiments are presented in Fig. 4a and 4b, which show the dispersion radius and instantaneous transport front velocity as a function of time for different voltages. In all these cases the front was tracked to a distance of 500 μm, limited by the field of view of our microscope. As can be seen, there exists an extremely strong dependence of the system dispersion on the applied electrokinetic potential, with the 4.0 V case representing an average of a 15 fold improvement in both front velocity and dispersion radius over the 3.0 V case. A detailed analysis of the superposition and relative importance of the electroosmotically induced convection and electrophoretic transport during the ejection process is provided in the "Characterization of electrokinetic transport" section below.

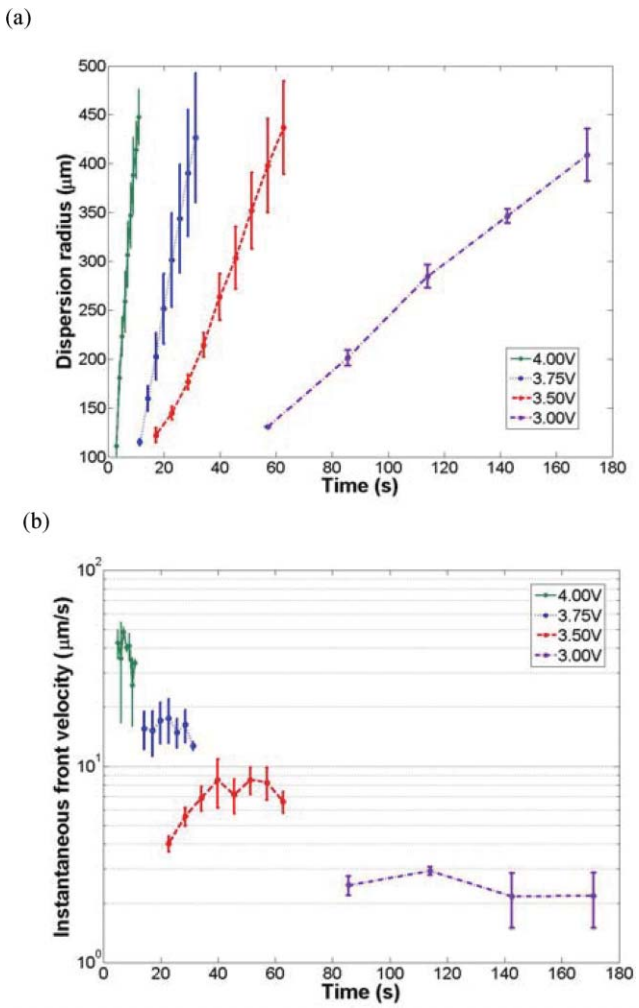

Fig. 4 (a) Dispersion radius *vs.* time for different applied potentials. (b) Instantaneous front velocity as a function of time.

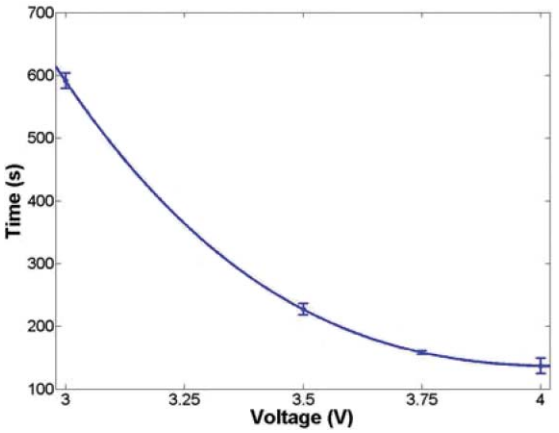

Fig. 5 Time required to completely empty the contents of the microwell as a function of applied potential.

The time required to empty the microwell of its original contents is plotted in Fig. 5, again as a function of applied potential. The well was determined to be empty when fluorescent tracer particles could no longer be seen exiting the well. As can be seen at 3.0 V, roughly 10 min was required to completely exchange the contents, which was reduced to just over 2 min at 4.0 V. Earlier diffusion based approaches required several hours[22–24] to completely eject the contents and thus, for cases where rapid on-command chemical delivery is required, this represents an improvement on the order of approximately 130 fold.

As is apparent from the above, in addition to reducing the overall ejection time, the electrokinetic technique also provides a method for controllably modulating the delivery rate through simple adjustment of the applied potential. While some existing transdermal microneedle systems[33] also posses this capability, the simplicity of the fabrication, assembly and operation (no fragile or moving parts nor complex or pulsatile pumping procedures) suggest that this approach may be more robust. The approach presented fuses the advantages of microwell devices, in terms of simplicity and storage stability, with the delivery flexibility afforded by microneedle systems.

Power consumption

As mentioned in the introduction, one of the most significant limitations to the development of autonomous microsystems is the relatively small amount of energy which can be stored, and voltage which can be generated, with existing battery technology. As such, minimizing voltage, power and energy requirements becomes a critical aspect of sub-component design. The small distance over which the potential is applied allows us to generate high field strengths (and therefore rapid electrokinetic transport), without the need for large applied potentials. To determine the power requirements and energy consumption of both the membrane dissolution and electrokinetic ejection stages used here, a Keithley 236 Source-Measure Unit was used to monitor the current load. Over the course of the 7 s required to dissolve the membrane at an applied potential of 5.0 V, an average power load of 3.70 mW

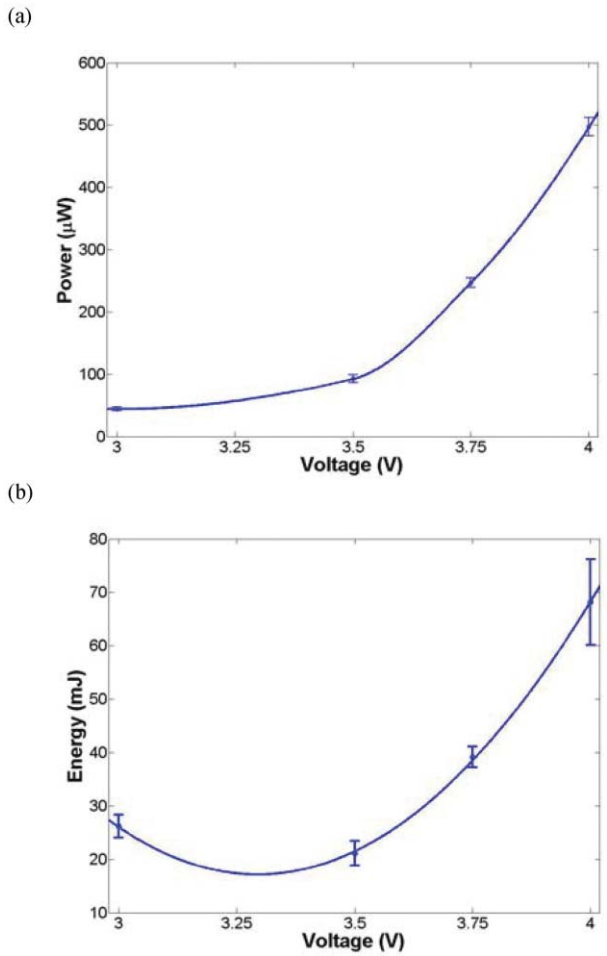

Fig. 6 (a) Average power load during ejection process. (b) Total energy consumed to completely empty the well using the times from Fig. 5. The line through the data points in this Figure represents a quadratic best fit.

was recorded, resulting in 26 mJ of energy consumed. Fig. 6 plots the power load (a) and energy consumption (b) for the same ejection voltages used in Fig. 4. The energy consumption was obtained by multiplying the average power load (Fig. 6a) by the time required to completely empty the well (Fig. 5). As can be seen for 3.0 V, an average power load of 44 μW was measured, resulting in a total energy consumption of 26 mJ. By comparison, at 4.0 V the average power load was 497 μW, resulting in 68 mJ of energy consumed. As can be seen from Fig. 6b, which plots the total energy required to empty the well as a function of applied voltage, there exists a clear minimum of around 20 mJ in the region between 3.0 V and 3.5 V. Note that this minimum is based on an interpolation of the quadratic curve fit used in Fig. 6b. The lowest actual measured power consumption was 22 mJ at 3.5 V. Although not optimal for rapid delivery, this region would be the best operational zone for low energy consumption. As can be seen from Fig. 6a, the power load begins the increase quite dramatically after 3.5 V. This is partially due to the fact that power should vary with the square of the applied voltage (for fixed resistance), however, there is also likely additional effects which contribute, like ohmic heating. Ohmic heating would serve to

Table 1 Comparison of power consumption of dosing systems

Working principle	Voltage/V	Power/mW
Electrostatic micropump[35]	200	1
Thermo-pneumatic[36]	15	450
Magnetohydrodynamic micropump[37]	10	18
Bubble-type planar micropump[38]	40	1000
Ionic conductive polymer film Micropump[39]	1.5	180
Electroactive microwell	**4**	**0.5**

decrease the well's resistivity and therefore increase the current load on the system, resulting in a larger than squared dependence on applied voltage. The minimum energy load region observed here represents the regime before the power load begins to spike and after the time required to empty the well has begun to drastically decrease from that observed at lower applied potentials.

For comparison, representative existing drug delivery dosing actuation systems[34] are shown in Table 1. As can be seen, they typically require on the order of 100 s of mW for operation or relatively high voltage. The device presented here represents a good combination of low voltage requirements and power draw. Based on these results the electroactive microwell system developed here appears to be a good candidate for adding drug delivery functionality to next generation autonomous microsystems.

Characterization of electrokinetic transport

To characterize the various electrokinetic transport processes involved in the ejection stage, a three-dimensional finite element model (FEM) of the system was constructed. The computational domain used here matched exactly that shown in Fig. 1a, comprising of both the well and a large exterior domain selected to be large enough to mimic the external environment. For reasons that will be expanded on later, the upper electrodes were also incorporated into the model.

Details of the modelling procedures and general assumptions are available in earlier works[40] and thus here we focus on the specifics of this implementation. For the purposes of this model, we assume that the solution's electrical and thermophysical properties are the same inside and outside the well and thus the applied potential field, ϕ, can be modelled with a simple Laplacian

$$\nabla^2\phi = 0 \tag{1}$$

Matching the experimental conditions as closely as possible, cathodic potentials were applied along the upper electrode and a ground (0 V) potential was set along the bottom of the well. With the exception of the electrode domains, electrical insulation conditions were applied along all other boundaries ($\partial\phi/\partial\boldsymbol{n} = 0$, where $\boldsymbol{n}$ is the surface normal). Fig. 7 illustrates the potential field lines obtained from these simulations. All calculations shown here and below were implemented using the COMSOL finite element package.

The electroosmotic flow field, $\boldsymbol{v}$, was computed by solving the low Reynolds number incompressible Stokes flow equations,

$$\eta\nabla^2\boldsymbol{v} - \nabla p = 0 \tag{2a}$$

$$\nabla\cdot\boldsymbol{v} = 0 \tag{2b}$$

(where η is the viscosity and p is the pressure) subject to electroosmotic slip, v_{eo}, conditions at the four walls of the microwell and the top surface of the device. The slip velocity was calculated using the Helmholtz–Smoluchowski equation $v_{eo} = -\varepsilon\zeta E/\eta$, where ε is the permittivity of the medium, ζ is the surface zeta potential and E is the field strength ($\boldsymbol{E} = -\nabla\phi$) evaluated tangential to the boundary. For the purposes of these simulations $\zeta = -60$ mV was used, as has been reported for silicon dioxide surfaces under similar electrolyte conditions to those used in our experiments,[39] due to the expected growth of a native oxide layer on the silicon after exposure to air. The remaining surfaces were assigned free slip ($\partial\boldsymbol{v}/\partial\boldsymbol{\tau} = 0$, where $\boldsymbol{\tau}$ is the tangential to the surface), zero penetration ($\boldsymbol{v}\cdot\boldsymbol{n} = 0$) boundary conditions.

Transient species transport was modelled using the modified convection diffusion equation,

$$\frac{\partial c}{\partial t} = D\nabla^2 c - \left(\boldsymbol{v} + \boldsymbol{v}_{ep}\right)\cdot\nabla c \tag{3}$$

where c is the local species concentration, t is the time and D is the diffusion coefficient. The convective component from eqn (3) comprises of both the bulk electroosmotic flow, $\boldsymbol{v}$ from eqn (2a), and the electrophoretic velocity of the transported species evaluated using $\boldsymbol{v}_{ep} = \mu_{ep}\boldsymbol{E}$, where μ_{ep} is the electrophoretic mobility. For the polystyrene fluorescent microspheres used here, the electrophoretic mobility was computed using $\mu_{ep} = \varepsilon\zeta/\eta$ with $\zeta = -40$ mV.[41]

Fig. 8 shows a two dimensional cut view of the electrical potential distribution and transport streamlines ($\boldsymbol{v} + \boldsymbol{v}_{ep}$) during the ejection process. To better understand the ejection process we consider two cases: Fig. 8a, pure electroosmotic flow, and Fig. 8b, both electroosmotic and electrophoretic components. From Fig. 8a it can be seen that the applied potential induces a strong electroosmotic flow component very near the wall, dragging fluid from the external environment

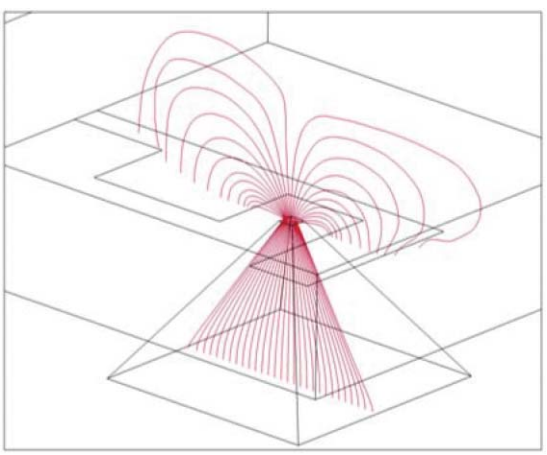

Fig. 7 Computed electric field lines in electroactive microwell.

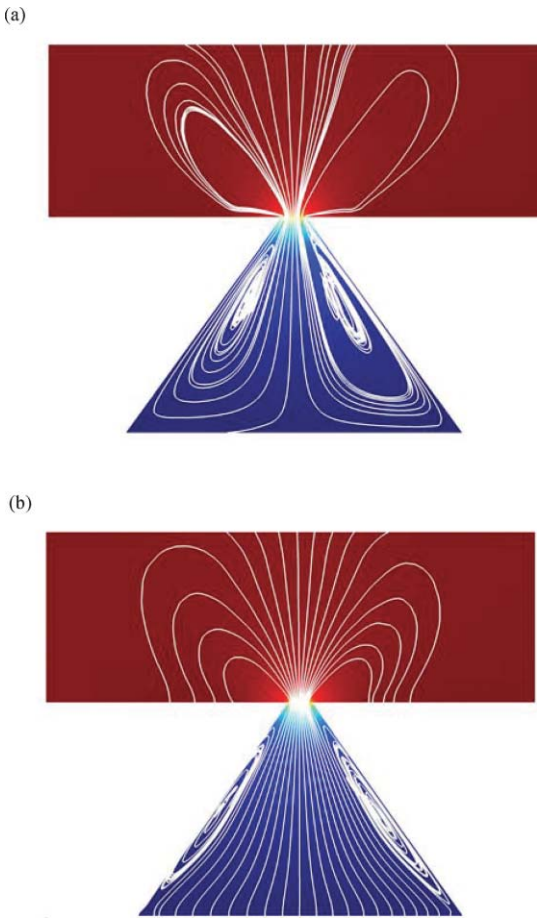

Fig. 8 Finite element simulations of the transport process. (a) Transport streamlines for pure electroosmosis. (b) Streamlines when all electrokinetic effects are considered. Colour contours show applied potential ranging from blue (ground) to red (maximum potential).

into the well. This then displaces the contents of the well, which is ejected through the middle of the outlet. The dragging of the fluid from the external environment back into the well is demonstrated experimentally in the second supplemental movie (movie2.wmv).† In this movie the motion of the tracer particles back into the well is clearly illustrated, suggesting the flow mechanism described above is qualitatively accurate.

This is also illustrated in Fig. 9a, which plots the transient convection–diffusion solution, eqn (3), in the well for a species with a diffusion coefficient equivalent to that of the polystyrene spheres used in the experiment and an applied potential of 3.5 V. When the electrophoretic component is included, Fig. 8b, the electroosmotic recirculation regions become confined to an area very near the wall. This is reflected in Fig. 9b, where the much more rapid ejection of the contents is apparent, since the electrophoretic ejection process dominates. Note that while the majority of the well contents are emptied after 25 s, the electroosmotic flow tends to pull back into the well some of the ejected species resulting in the more concentrated regions along the wall, most evident in the final two timeframes. This accounts for the experimental observation that while the initial dispersion occurs quite rapidly (Fig. 3), the amount of time to completely empty the well is much longer (Fig. 5). Since these simulations suggest that the majority of the contents are ejected during the first 20 s to 25 s the empty times shown in Fig. 5 represent an upper limit.

To further validate the numerical results, we compare the dispersion radius measured experimentally with that obtained from the simulations shown in Fig. 9b. The results are shown in Fig. 10 for the 3.5 V case. As can be seen, the trends between the two cases are very similar, with the numerical results tending to over-predict the dispersion radius over the first 8 s of the process. The reason for this is likely due to uncertainties in the electrophoretic mobility of the polystyrene beads in the buffer solution used here and an over estimate of the applied potential (we ignored any potential drops along the leads or at the solution–electrode interface). In general, however, neither of these would affect the overall transport mechanisms described above.

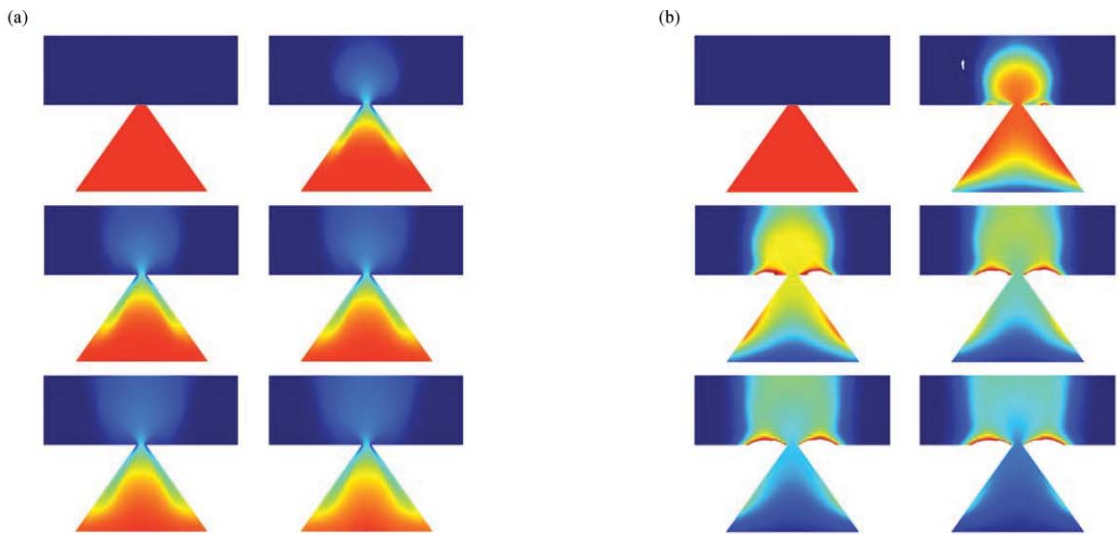

Fig. 9 Finite element analysis of time-dependent species transport. Images show cut view of species concentration every 5 s up to 25 s after the ejection process (a) electroosmosis only (b) electrophoresis and electroosmosis.

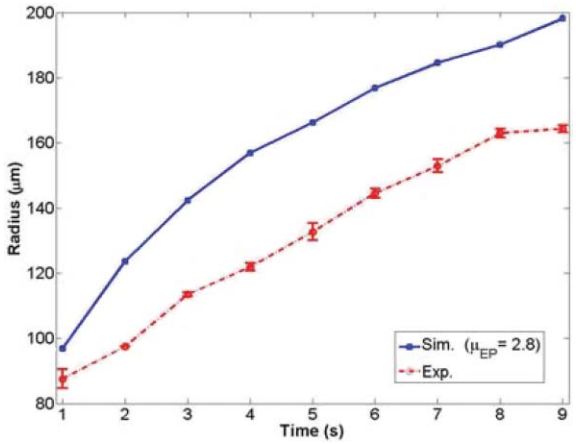

Fig. 10 Plot comparing experimental and numerical results on the 3.5 V case.

Summary and conclusion

We have demonstrated here an implantable, low power and rate controllable drug delivery device incorporating an electroactive microwell structure. This approach serves to actively repel the drugs inside the well using a combination of electroosmotic and electrophoretic effects, which are controlled through an electric potential applied between the top and bottom of the well. The contents dispersal rate and energetic consumption of the device were characterized experimentally. It was found that the ejection process could be completed in less than 2 minutes or using as little as 20 mJ of energy, both of which compared favourably to the state of the art microsystems. Detailed 3D numerical simulations were used to model the electrokinetic transport involved in the ejection process. In addition to providing a physical insight in to the transport mechanism, the simulations revealed that the majority of the contents are ejected early in the process.

Acknowledgements

This work was supported by the Defense Advanced Research Project Agency, Microsystems Technology Office, Hybrid Insect MEMS (HI-MEMS) program, through the Boyce Thompson Institute for Plant Research. Distribution unlimited. Fundamental research exempts from prepublication controls. We would also like to acknowledge helpful discussions from Bernardo Cordovez and Likun Chen.

References

1 M. Tanaka, An industrial and applied review of new MEMS devices features, *Microelectron. Eng.*, 2007, **84**, 1341.
2 M. Gad-el-Hak, in *MEMS: design and fabrication*, CRC/Taylor & Francis Group, Boca Raton, FL, 2006.
3 S. P. Beeby, M. J. Tudor and N. M. White, Energy harvesting vibration sources for microsystems applications, *Meas. Sci. Technol.*, 2006, **17**, R175.
4 B. Warneke, M. Last, B. Liebowitz and K. S. J. Pister, Smart dust: Communicating with a cubic-millimeter computer, *Computer*, 2001, **34**, 44.
5 R. Bashir, D. Akin, R. Gómez, H. Li, W.-J. Chang and A. Gupta, From bioMEMS to bionanotechnology: Integrated biochips for the detection of cells and microorganisms, *Proc. Mater. Res. Soc.*, 2003, **773**, 911.
6 S. Bhattacharya, J. S. Jang, L. J. Yang, D. Akin and R. Bashir, Biomems and nanotechnology-based approaches for rapid detection of biological entities, *J. Rapid Methods Autom. Microbiol.*, 2007, **15**, 1.
7 B. Bhushan, Nanotribology and nanomechanics of MEMS/NEMS and BioMEMS/BioNEMS materials and devices, *Microelectron. Eng.*, 2007, **84**, 387.
8 M. Madou, J. Zoval, G. Y. Jia, H. Kido, J. Kim and N. Kim, Lab on a CD, *Annu. Rev. Biomed. Eng.*, 2006, **8**, 601.
9 P. S. Dittrich and A. Manz, Lab-on-chip: microfluidics in drug discovery, *Nat. Rev. Drug Discovery*, 2006, **5**, 211.
10 D. Erickson and D. Li, Integrated microfluidic devices, *Anal. Chem. Acta*, 2004, **507**, 11.
11 P. Abgrall and A. M. Gue, Lab-on-chip technologies: making a microfluidic network and coupling it into a complete microsystem – a review, *J. Micromech. Microeng.*, 2007, **17**, R15.
12 C. Q. Yi, C. W. Li, S. L. Ji and M. S. Yang, Microfluidics technology for manipulation and analysis of biological cells, *Anal. Chem. Acta*, 2006, **560**, 1.
13 A. R. Eliakim, Video capsule endoscopy of the small bowel (PillCam SB), *Curr. Opin. Gastroenterol.*, 2006, **22**, 124.
14 R. Dickman and R. Fass, Ambulatory esophageal pH monitoring: new directions, *Dig. Dis.*, 2006, **24**, 313.
15 G. Orive, R. M. Hernandez, A. R. Gascon, A. Dominguez-Gil and J. L. Pedraz, Drug delivery in biotechnology: present and future, *Curr. Opin. Biotechnol.*, 2003, **14**, 659.
16 J. M. Maloney, S. A. Uhland, B. F. Polito, N. F. Sheppard, Jr., C. M. Pelta and J. T. Santini, Jr., Electrothermally activated microchips for implantable drug delivery and biosensing, *J. Controlled Release*, 2005, **109**, 244.
17 A. Ahmed, C. Bonner and T. A. Desai, Bioadhesive microdevices with multiple reservoirs: a new platform for oral drug delivery, *J. Controlled Release*, 2002, **81**, 291.
18 A. C. Grayson, R. S. Shawgo, A. M. Johnson, N. T. Flynn, Y. Li, M. J. Cima and R. Langer, A BioMEMS Review: MEMS Technology for physiologically integrated devices, *Proc. IEEE*, 2004, **92**, 6.
19 M. S. Kim, K. S. Seo, H. Hyun, S. K. Kim, G. Khang and H. B. Lee, Sustained release of bovine serum albumin using implantable wafers prepared by MPEG-PLGA diblock copolymers, *Int. J. Pharm.*, 2005, **304**, 165.
20 Physician's Desk Reference, ed. R. Arky, Medical Economics Company, Montvale, NJ, USA, 1998, pp. 2587.
21 Physician's Desk Reference, ed. R. Arky, Medical Economics Company, Montvale, NJ, USA, 1998, pp. 3139.
22 J. T. Santini, Jr., M. J. Cima and R. Langer, A controlled-release microchip, *Nature*, 1999, **397**, 335.
23 R. A. Scheidt, J. T. Santini, A. C. Richards, A. M. Johnson, A. Rosenberg, M. J. Cima and R. Langer, Microchips as implantable drug delivery devices, *Proc. Annu. Int. IEEE-EMBS Special Topic Conf. Microtechnol. Med. Biol.*, 2000, 483.
24 J. T. Santini, Jr., A. C. Richards, R. S. Scheidt, M. J. Cima and R. Langer, Microchips as controlled drug-delivery devices, *Angew. Chem., Int. Ed.*, 2000, **39**, 2396.
25 B. Cordovez, D. Psaltis and D. Erickson, Trapping and storage of particles in electroactive microwells, *Appl. Phys. Lett.*, 2007, **90**, 024102.
26 K. J. Lee, K. A. Tosser and R. G. Nuzzo, Fabrication of stable metallic patterns embedded in poly (dimethylsiloxane) and model application in non-planar electronic and lab-on-a-chip device patterning, *Adv. Funct. Mater.*, 2005, **15**, 557.
27 T. G. I. Ling, M. Beck, R. Bunk, E. Forsen, J. O. Tegenfeldt, A. A. Zakharov and L. Montelius, Fabrication and characterization of a molecular adhesive layer for micro- and nanofabricated electrochemical electrodes, *Microelectron. Eng.*, 2003, **67**, 887.
28 E. J. Fitzsimons and J. Sendroy, Jr., Distribution of electrolytes in human blood, *J. Biol. Chem.*, 1961, **236**, 1595.
29 R. P. Frankenthal and D. J. Siconolfi, The anodic corrosion of gold in concentrated chloride solutions, *J. Electrochem. Soc.*, 1982, **6**, 1192.
30 G. Voskerician, M. S. Shive, R. S. Shawgo, H. von Recum, J. M. Anderson, M. J. Cima and R. Langer, Biocompatibility

and biofouling of MEMS drug delivery devices, *Biomaterials*, 2003, **24**, 1959.
31 R. R. J. Richardson, J. A. Miller and W. M. Reichert, Polyimides as biomaterials - preliminary biocompatibility testing, *Biomaterials*, 1993, **14**, 627.
32 M. C. Belanger and Y. Marois, Hemocompatibility, biocompatibility, inflammatory and in vivo studies of primary reference materials low-density polyethylene and polydimethylsiloxane: A review, *J. Biomed. Mater. Res.*, 2001, **58**, 467.
33 S. Henry, D. V. McAllister, M. G. Allen and M. R. Prausnitz, Microfabricated microneedles: a novel approach to transdermal drug delivery, *J. Pharm. Sci.*, 1998, **87**, 922.
34 N. Tsai and C. Sue, Review of MEMS-based drug delivery and dosing systems, *Sens. Actuators, A*, 2007, **134**, 555.
35 R. Zengerle, J. Ulrich, S. Kluge, M. Richter and A. Richter, A bidirectional silicon micropump, *Sens. Actuators, A*, 1995, **50**, 81.
36 W. K. Schomburg, J. Vollmer, B. Bustgens, J. Fahrenberg, H. Hein and W. Menz, Microfluidic components in LIGA technique, *J. Micromech. Microeng.*, 1994, **4**, 186.
37 J. Jang and S. S. Lee, Theoretical and experimental study of MHD (magnetohydrodynamic) micropump, *Sens. Actuators, A*, 2000, **80**, 84.
38 J. D. Zahn, A. Deshmukh, A. P. Pisano and D. Liepmann, Continuous on-chip for microneedle enhanced drug delivery, *Biomed. Microdev.*, 2004, **6**, 183.
39 S. Guo and T. Fukuda, Development of the micro pump using ICPF actuator, *Proc. IEEE Int. Conf. Robotics Autom.*, 1997, **1**, 266.
40 D. Erickson and D. Li, Microscale flow and transport simulation for electrokinetic and lab-on-chip applications, in *Biomems and biomedical nanotechnology*, ed. R. Bashir and S. Wereley, Kluwer Academic Publishing, New York, NY, 2006, vol. 4.
41 B. J. Kirby and E. F. Hasselbrink, Jr., Zeta potential of microfluidic substrates: 2. Data for polymers, *Electrophoresis*, 2004, **25**, 203.

